Dalton Transactions

PAPER

View Article Online
View Journal

Cite this: DOI: 10.1039/c5dt02471d

Grafting transition metal–organophosphonate fragments onto heteropolyoxomolybdate: activity in photocatalysis†

Xiaopeng Sun, Zhijie Liang, Pengtao Ma, Ran Ban, Mingshuang Jiang, Dongdi Zhang,* Jingping Wang and Jingyang Niu*

Received 30th June 2015,
Accepted 7th September 2015

DOI: 10.1039/c5dt02471d

www.rsc.org/dalton

A novel organophosphonate-functionalized heteropolyoxomolybdate incorporated nickel cluster, $CsNa_9[H_2\{Ni_3O_2(H_2O)_6\}(PMo_6O_{21})_2\{Ni(OOCCH_2NHCH_2PO_3)_2\}_3]\cdot 21H_2O$ (**1**), has been synthesized, which represents the first member of the family of oxomolybdenum organophosphonate containing hexanuclear Ni(II) in a polyanion framework. The polyanion comprises a unique ladder-type $\{Ni_3O_{10}(H_2O)_6\}$ cluster and three $\{Ni(OOCCH_2NHCH_2PO_3)_2\}$ bridgings, which are capped on either end by a $\{PMo_6O_{28}\}$ group. Photocatalytic experiments indicate that **1** exhibits catalytic activity for the photodegradation of RhB solution. Furthermore, magnetic studies indicate that **1** displays antiferromagnetic interactions.

Introduction

The oxomolybdenum organophosphonate family (Mo/O/RPO_3^{2-}) has been the subject of great efforts not only due to the extended structures with great versatility in size, shape and nuclearity but also because of the potential applications in photochromism, electrochemistry, medicine, magnetism and catalysis.[1] To date, the field has produced a large number of species. Examples of such kinds of Mo/O/RPO_3^{2-} are the organomonophosphonate derivatives, $[(RPO_3)_2Mo_5O_{15}]^{4-}$ (R = CH_3, C_2H_5, C_6H_5, $C_2H_4NH_3^+$, $CH_2C_6H_4NH_3^+$, $CH_3CHNH_3^+$ and $CH_3CH(CH_3)CHNH_3^+$);[2] organodiphosphonate derivatives, $\{(O_3PCH_2PO_3)Mo_2O_4\}$,[3a] $\{(O_3PC_2H_4PO_3)Mo_2O_5\}$,[3b] $\{O_3P(CH_2)_n$-$PO_3Mo_5O_{15}\}$ (n = 2, 3, 4),[3c,d] $\{(O_3P(CH_2)_5PO_3)Mo_6O_{18}\}$,[3e] $\{(O_3PCH_2PO_3)Mo_6O_{22}\}$,[3f] $\{(O_3PCH_2PO_3)_3Mo_7O_{16}\}$,[3g] $\{(Mo_3O_8)_2O$-$(O_3PCRPO_3)_2\}$ (R = $CH_2S(CH_3)_2$, $C_4H_5N_2$) and $\{MoO_2(O_3PCR$-$(OH)PO_3)_2\}$ (R = $C_3H_6NH_2$);[3h] organotriphosphonate derivatives, $\{[N(CH_2PO_3)_3]Mo_6O_{16}(OH)(H_2O)_4\}$;[4] phosphonocarboxylate derivatives, $\{(O_2CCH_2PO_3)_2Mo_5O_{15}\}$,[5a] $\{(HOOCC_2H_4PO_3)_2$-$Mo_5O_{15}\}$,[5b] $\{(HOOCC_5H_9NCH_2PO_3)_2Mo_5O_{15}\}$,[5c] $\{(HO_2CC_6H_4PO_3)$-$Mo_2O_6\}$, $\{(O_2CC_6H_4PO_3)_2Mo_5O_{15}\}$, $\{(O_2CC_6H_4PO_3)MoO_2F\}$ and $\{(HO_2CC_6H_4PO_3)_2Mo_{12}F_4O_{34}(H_2O)_4\}$.[5d] On the other hand, most reported transition metals (TMs) contained in Mo/O/RPO_3^{2-} derivatives serve as the cationic component, such as $[Co_3(bipy)_4]^{6+}$ and $[Cu(bipy)]^{2+}$ (bipy = 4,4′-bipyridine);[5b] $[Cu(bpy)]^{2+}$, $[Co(bpy)_3]^{2+}$ $[Co(terpy)_2]^{3+}$, $[Ni(phen)_2]^{2+}$ and $\{Cu(phen)\}^{2+}$ (bpy = 2,2′-bipyridine, phen = *o*-phenanthroline, terpy = 2,2′:6,2″-terpyridine);[5d] $\{Ni_2(bpyr)\}^{4+}$ and $\{Cu_2(bpyr)_n\}^{4+}$ (n = 1, 2, bpyr = bipyrimidine);[6a] $\{Cu_2(tpypyz)\}^{4+}$ (tpypyz = tetra-2-pyridylpyrazine);[6b] $[Co_2(tpypyz)]^{4+}$ and $[Ni_2(tpypyz)]^{4+}$.[3e]

However, only one report concerned the Mo/O/RPO_3^{2-} framework with the covalent interactions of Mn,[7] and the TMs in a polyanion framework usually show useful properties, such as magnetism, redox behavior and catalysis, *etc*. Thus, the incorporation of a TM into Mo/O/RPO_3^{2-} is a crucial step in the design and synthesis of novel clusters with excellent potential applications. Among the various 3d TM ions, the Ni^{II} ion first seizes our attention owing to its flexible coordination modes, for instance, square, trigonal bipyramid, square pyramid and octahedron. Moreover, polyoxomolybdates attract our interest based on the activity in degradation of organic dyes.[8]

As a phosphonocarboxylate, glyphosate (H_3L = $HOOCCH_2$-$NHCH_2PO_3H_2$) displays three pertinent features: (1) the multidentate ligand H_3L functionalized with amine, carboxylate and phosphonate groups exhibits many coordination modes, resulting in various interesting structures. (2) It can show varying degrees of deprotonation just by changing the pH of the reaction medium.[9] (3) The results of ^1H, ^{13}C and ^{31}P NMR spectroscopy depict that the carboxylate, the phosphonate and the amine are deprotonated, gradually.[10]

Henan Key Laboratory of Polyoxometalate Chemistry, Institute of Molecular and Crystal Engineering, College of Chemistry and Chemical Engineering, Henan University, Kaifeng 475004, Henan, China. E-mail: ddzhang@henu.edu.cn, jyniu@henu.edu.cn; Fax: (+86) 371-23886876

†Electronic supplementary information (ESI) available: IR spectra, XRPD pattern and TGA of **1** (Fig. S1, S2 and S4); the synthetic pathway of **1** (Fig. S3); BVS of Mo, Ni, P and O atoms in **1a** (Fig. S5, Tables S1–S4); crystallographic data of **1** (Table S5); selected bond angles (°) of **1** (Table S6); some structural figures (Fig. S6–S9) and the additional photocatalysis related table and figure (Fig. S10 and Table S7). CCDC 1057128. For ESI and crystallographic data in CIF or other electronic format see DOI: 10.1039/c5dt02471d

Herein, we present a new H_3L-based heteropolyoxomolybdate containing hexa-nuclear Ni(II) $CsNa_9[H_2\{Ni_3O_2(H_2O)_6\}(PMo_6O_{21})_2(NiL_2)_3]\cdot 21H_2O$ (L = $OOCCH_2NHCH_2PO_3$) (**1**), which was synthesized by the reaction of a three-component system consisting of a phosphoric molybdenum oxide cluster as precursor, an organic component and a secondary metal ion as bridging fragments. Besides, it was confirmed by single crystal X-ray diffraction, X-ray powder diffraction, elemental analyses, thermogravimetric analyses, X-ray photoelectron spectroscopy, IR and UV-vis spectra.

As far as we know, it is the first example of heteropolyoxomolybdates functionalized with six nickel atoms and six phosphonocarboxylate fragments, simultaneously.

Results and discussion

Synthesis

Compared with the noncovalent polyoxometalate (POM)-based derivatives, hybrids with covalent interactions between POMs and organic groups have been far less explored. Furthermore, organophosphonate ligands and TM synchronously incorporated into the framework of POMs are rare.[11,12] The covalent combination of POMs with TM, as well as organophosphonate groups, could improve the directionality and synergetic effect between inorganic and organic components, that exactly grabs our attention. Compound **1** was prepared by the reaction of $Na_2HPMo_{12}O_{40}\cdot 14H_2O$ (noted as $\{PMo_{12}\}$), H_3L and $NiCl_2\cdot 6H_2O$ with a molar ratio of 2 : 7 : 4 in 80 °C aqueous solution under stirring for 2 h in the presence of Cs^+. Notably, the pH of the reaction system is the key factor influencing the isolation and quality of the crystals. The optimal pH range of the reaction is from 5.8 to 6.5. For a lower pH (pH < 5.8), no crystal was formed; for a higher pH (pH > 6.5), the crystal quality of **1** was poor and the yield was reduced. Except for the vital factor of pH, many parallel experiments indicated that the significance in the formation of the compound was the introduction of nickel. In fact, to find "pure" Mo/O/RPO_3^{2-} building blocks, we conducted a similar one-pot reaction in the absence of nickel, and to our regret we did not gain the desired product. In addition, the single-crystal samples of **1** could be obtained from 70 to 90 °C.

Structural descriptions

Single-crystal X-ray structural analysis reveals that compound **1** crystallizes in the monoclinic space group *C*2/*c* and consists of a cesium cation, nine sodium cations, twenty-one water molecules of crystallization and the polyanion $[H_2\{Ni_3O_2(H_2O)_6\}(PMo_6O_{21})_2(NiL_2)_3]^{10-}$ (**1a**) (top in Scheme 1). In particular, each of the six H_3L molecules joins two edge-sharing Mo centers *via* the functional phosphate above or below the $\{PMo_6O_{28}\}$ group, which leads to two opposite $\{(PMo_6O_{22})L_3\}$ (right in Scheme 1) building blocks. The same repeating structural subunits $\{(PMo_6O_{22})L_3\}$ are linked into the larger architecture $\{(PMo_6O_{22})_2(NiL_2)_3\}$ (Fig. S6a†) by three distorted NiO_4N_2 octahedra that differ from the reported coordination of the NiO_6 octahedron.[13] The covalent interactions of the ladder-type linkage $\{Ni_3O_{10}(H_2O)_6\}$ (left bottom in Scheme 1) with three bow-tie shaped $\{NiO_4\}$ fragments (Fig. 1b) furnish a significant step to the production of polyanion **1a**. As known, two opposite $\{PMo_6O_{28}\}$ (bottom in Scheme 1) capping groups are connected by such a ladder-type $\{Ni_3O_{10}(H_2O)_6\}$ cluster forming the $\{Ni_3O_2(H_2O)_6(PMo_6O_{24})_2(\mu_3\text{-}O)_2(\mu_2\text{-}O)_6\}$ framework with a "Z-shaped" skeleton (left in Scheme 1), which has never been reported. The difference in organic components reduces the overall symmetry of the molecule from C_{3v} of the framework $[RPMo_6O_{21}(O_2CCH_2NH_3)_3]^{2-}$ (R = OH, CH_3, C_2H_5, H) that has been reported by Kortz[14] to C_3 of $\{(PMo_6O_{22})L_3\}$. It should be noted that two μ_2-O atoms of each PO_3 group connect two

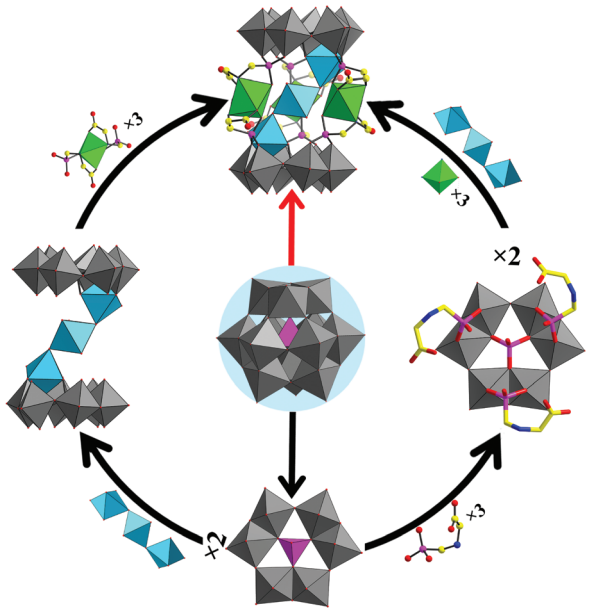

Scheme 1 Representation of the assembly of polyanion **1a**. The red route shows the direct one-pot synthesis and the black routes give the imaging stepwise methods. Color code: $\{MoO_6\}$, grey octahedral; $\{NiO_4N_2\}$, green octahedral; $\{NiO_6\}$, sky blue octahedral; P (pink); N (blue); C (yellow); O (red). The H atoms are omitted for clarity.

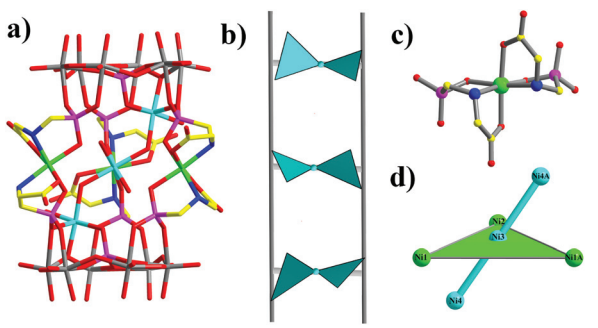

Fig. 1 (a) Stick representation of polyanion **1a**; (b) schematic of the ladder-type linking bridge; (c) ball-and-stick view of $\{NiL_2\}$; (d) the relative position of hexa-nuclear Ni(II) cluster.

edge-sharing MoO_6 octahedra and the other μ_2-O atom binds to a Ni atom, which is coordinated to two N atoms, two {COO} and two $\{PO_3\}$ groups from two H_3L molecules generating a $\{NiL_2\}$ backbone (Fig. 1c). Compared with the reported local structure CdL,[15] polyanion **1a** can be seen as a structural unit formed by three isolated NiL_2 based on the "Z-shaped" framework $\{Ni_3O_2(H_2O)_6(PMo_6O_{24})_2(\mu_3\text{-}O)_2(\mu_2\text{-}O)_6\}$. Therefore, the H_3L ligand acts as a stanchion in the formation of the organophosphonate-decorated TM-contained polyoxomolybdate frameworks.

All of the four crystallographically independent nickel ions (Ni1, Ni2, Ni3 and Ni4) in **1** adopt distorted octahedral geometries. With the decoration of a pair of H_3L ligands, the Ni1 and Ni2 atoms are defined by two N atoms [Ni–N, 2.102(6)–2.141(6) Å] and four O atoms from {COO} and $\{PO_3\}$ groups, respectively [Ni–O_{COO}, 2.030(6)–2.054(5) Å; Ni–O_{PO3}, 2.081(5)–2.092(4) Å]. Interestingly, a normative isosceles triangle is constructed by Ni1, Ni1A and Ni2 atoms with the base line 7.481(13) Å between Ni1 and Ni1A atoms, the two equal sides 7.858(15) Å and the basic angle is 61.576(10)° (Fig. S7a†). In $\{Ni_3(H_2O)_2(\mu_3\text{-}O)_2(\mu_2\text{-}O)_2\}$, the coordination sites of the Ni3 atom are occupied by two terminal O atoms belonging to the coordinated water molecules [Ni3–O_w, 2.024(5) Å], two μ_3-O atoms from a pair of $\{PO_3\}$ groups [Ni3–μ_3-O, 2.054(5) Å], as well as two μ_2-O groups bridging with Ni4 and Ni4A [Ni3–μ_2-O, 2.140(5) Å]. Compared with the Ni3 atom, the Ni4 atom in the local structure $\{Ni4(H_2O)(\mu_3\text{-}O)_3(\mu_2\text{-}O)_2\}$ is defined by the terminal O atom from the coordinated water molecule [Ni4–O_w, 2.084(6) Å], two μ_3-O atoms from two $\{PO_3\}$ groups coordinating to different Ni atoms [Ni4–μ_3-O, 2.034(5)–2.036(5) Å] and a μ_3-O atom in the corner of two MoO_6 octahedra [Ni4–μ_3-O, 2.057(5) Å], and two μ_2-O groups bridging with Ni3 and the central heteroatom P [Ni4–μ_2-O, 2.101(5)–2.105(4) Å]. Additionally, the three Ni atoms in the ladder-type $\{Ni_3O_{10}(H_2O)_6\}$ cluster are almost linear with the Ni4–Ni3–Ni4A angle of 174.96° (Fig. S7b†), and the angle between the Ni4–Ni3–Ni4A plane and the normative isosceles triangle is 56.12° (Fig. S8a†). Furthermore, the two planes formed by P2, P3, P4 and P2A, P3A, P4A are nearly paralleled with the dihedral plane angle 0.10° (Fig. S8b†).

Analyses of BVS, XPS, XRPD, TGA, IR and UV characterizations

Bond valence sum calculations and X-ray photoelectron spectroscopy. The BVS[16] values for Ni and Mo atoms are from 1.95 to 2.13 with an average of 2.02, and from 6.02 to 6.11 with an average of 6.05, respectively. These results indicate that all the Ni and Mo atoms are in the +2 and +6 oxidation states, respectively. The BVS values for the central heteroatoms P located slightly above/below the $\{Mo_6\}$ plane (Fig. S6b†) are 4.92, while the P atoms in H_3L ligands are in the 2.66–2.74 range with the average of 2.70, which confirms the assigned +5 and +3 oxidation states of P atoms. The oxidation states for Mo and P atoms are further confirmed by XPS spectra. In the XPS spectra, two peaks at 232.3 and 235.4 eV are assigned to Mo^{6+} ($3d_{5/2}$) and Mo^{6+} ($3d_{3/2}$), severally (Fig. 2a); and Fig. 2b shows two overlapped peaks at 132.3 eV and 133.6 eV with a peak

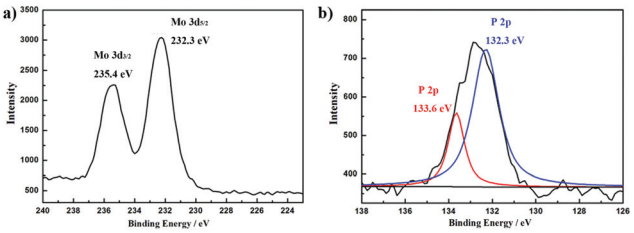

Fig. 2 (a) XPS spectra of **1** for Mo $3d_{5/2}$ and Mo $3d_{3/2}$, (b) XPS spectra of **1** for P_{2p}, showing the existence of mixed-valence P.

area ratio of 3 : 1, which can be attributed to P^{3+} and P^{5+}, respectively.[17a] In addition, considering the charge balance of compound **1**, eight protons need to be added. To locate the positions of these protons, BVS of all the O atoms on POM fragments are carried out and the BVS values for O38 (O38A, A: $2 - x, y, 0.5 - z$,), O39 (O39A) and O40 (O40A) are 0.368, 0.564 and 0.313 indicating that they are diprotonated (section 5 in ESI†). The remaining two protons are delocalized on the whole anion cluster, which is common in POM chemistry.[17b]

X-ray powder diffractograms. As shown in Fig. S2,† the diffraction peaks of both experimental and simulated patterns match well, indicating the good phase purity for **1**. The differences in intensity between the experimental and simulated XRPD patterns might be due to the variation in preferred orientation of the powder sample during collection of the experimental XRPD.

Thermogravimetric analyses. To investigate the thermal stability of compound **1**, thermogravimetric analyses (TGA) were performed under a nitrogen flow (Fig. S4†). The TG curve exhibits two steps of weight loss in the temperature range 25–900 °C. The first weight loss of 12.31% from 25 to 166 °C is attributed to twenty-one crystalline water molecules and six coordinated water molecules (calc. 11.88%). The rest of the observed weight loss (24.74%) is in agreement with the calculated value (24.93%), which occurs from 166 to 900 °C, mainly due to the escape of six NH_3, seven H_2O and eighteen CO_2 molecules.[18]

IR spectra. The IR spectrum of **1** shows the skeletal vibrations in the region between 500 and 1600 cm^{-1}, which is in good agreement with the result of single-crystal X-ray structural analysis. The terminal Mo–O_t vibrations are seen as prominent bands at 935 and 889 cm^{-1} and the strong peak at 677 cm^{-1} is assigned to Mo–O–Mo bridges vibrations. The characteristic peaks at 1016, 1067 and 1121 cm^{-1} are derived from P–O vibration. The broad peaks around 3492 cm^{-1} and 3375 cm^{-1} are attributed to the stretching modes of lattice and coordinated water molecules.[19] In addition, the signal appearing at 2918 cm^{-1} is assigned to the $\nu(CH_2)$ stretching vibration and the bands at 1583 and 1393 cm^{-1} are attributed to the carboxyl characteristic vibrations. In comparison with the uncoordinated phosphonocarboxylate (1700–1740 cm^{-1}), the ν(COO) vibrations of **1** are shifted to low frequency as a result of the carboxylate interaction with the metal ion,[20] which indicates the coupling of the {COO} group from H_3L (Fig. S1†).

UV spectra

The UV spectrum in aqueous solution in the range of 400–200 nm of compound **1** (2.5×10^{-5} mol L^{-1}) reveals two characteristic peaks: the lower energy absorption band centered at around 232 nm and the higher at 208 nm (Fig. 3a), which can be attributed to the pπ–dπ charge-transfer transition of the $O_{b,c} \rightarrow$ Mo bonds, and pπ–dπ charge-transfer transition of the $O_t \rightarrow$ Mo bonds, respectively.[21] Interestingly, compared with the two equivalent characteristic peaks at 246 and 214 nm of $\{PMo_{12}\}$ (2.5×10^{-5} mol L^{-1}), the bands of **1** show a blue shift which may be the result of the function of Ni centres and H_3L ligand in the polyanion structure.

As is well known, POMs are commonly sensitive to the pH value. In order to investigate the influence of the pH values on the stability of the compound in aqueous solution, **1** was elaborately probed by means of UV spectra. Diluted HCl and NaOH solution were used to adjust the pH values in the acidic direction and alkaline direction, respectively.

As shown in Fig. 3c and d, the UV spectra of **1** do not change at all even when the pH value has been increased to 10.48. However, the absorbance bands at 232 and 208 nm are gradually red-shifted and become weaker and weaker, suggesting the decomposition of the POM skeleton of **1** from the pH at 4.48. Additionally, the on-going spectroscopic measurement was performed in the aqueous system (Fig. 3b), and the unchanged position and strength of the absorption bands indicate that compound **1** may be stable in the aqueous system at ambient temperature for at least 18 hours.

Magnetic property

The variable temperature magnetic susceptibility of **1** has been investigated at 1000 Oe in the range of 1.8–300 K and is plotted in the form of χ_m *versus* T, $\chi_m T$ *versus* T and χ_m^{-1} *versus* T (inset), respectively (Fig. 4). The experimental $\chi_m T$ value at 300 K is 5.89 emu K mol^{-1}, which is close to the expected value for six uncoupled high-spin Ni^{2+} ions with 6.0 emu K mol^{-1} ($S = 1$ and $g = 2$). Upon cooling, the $\chi_m T$ values of **1** changed little until 30 K with the value 5.55 emu K mol^{-1}, then decreased sharply to reach 2.01 emu K mol^{-1} at 1.8 K.

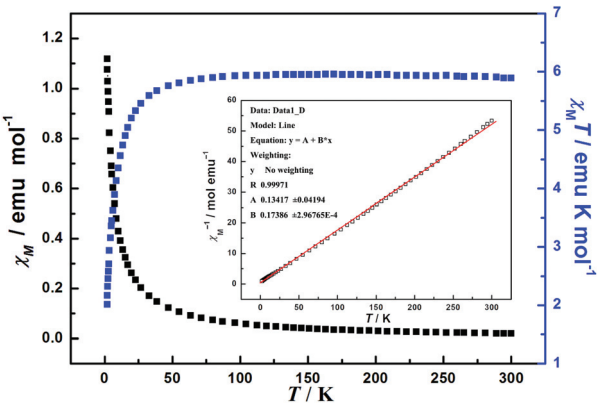

Fig. 4 Plots of χ_M and $\chi_M T$ *versus* T from 1.8 to 300 K for **1** at H = 1000 Oe. Inset figure: the χ_M^{-1} *versus* T curve and the linear fit of the temperature dependence of **1**.

This clearly shows the existence of the antiferromagnetic coupling interactions between adjacent Ni(II) centers as described by Kortz.[22] The temperature dependence of the reciprocal susceptibilities (χ_m^{-1}) obeys the Curie–Weiss law from 1.8 to 300 K with a negative Weiss constant $\theta = -0.77$ K, C = 5.75 emu K mol^{-1}, which further indicates that the magnetic property of **1** is dominated by the antiferromagnetic coupling in the cluster.

Photocatalytic activity

Rhodamine B (RhB) is often used as model of dye pollutant to evaluate the effectiveness of photocatalysts in the purification of waste water.[23] Compound **1** was added into a 40 mL aqueous solution of RhB (2.0×10^{-5} mol L^{-1}), and the obtained solution was magnetically stirred in the dark for about 30 min to ensure the equilibrium of the working solution. The stirring solution was then exposed to a 500 W Xe-lamp irradiation at a distance of 4–5 cm between the liquid surface and the lamp. The results indicate that **1** displays efficient photocatalytic activity for the conversion of RhB. The changes in the UV-vis absorption spectra of RhB solutions in the presence of **1** (Fig. 5a and S10†) show that the absorbance of RhB (λ = 553 nm) decreased along with the prolonged reaction time. Further, Fig. 5b shows the decrease of C_t/C_0 upon increasing the irradiation time from 0 to 3 h at the given time intervals (C_t, the RhB concentration after irradiation with time intervals; C_0, the RhB concentration before irradiation).

In contrast, the degradation reaction of RhB aqueous solution under the same conditions hardly happened in the blank experiment. In order to select the optimum usage amount of the photocatalyst, a series of experiments with constant concentration of RhB (C_0) solution were performed. The results of the incremental usage amount of **1** (0, 6.4×10^{-7}, 1.28×10^{-6},

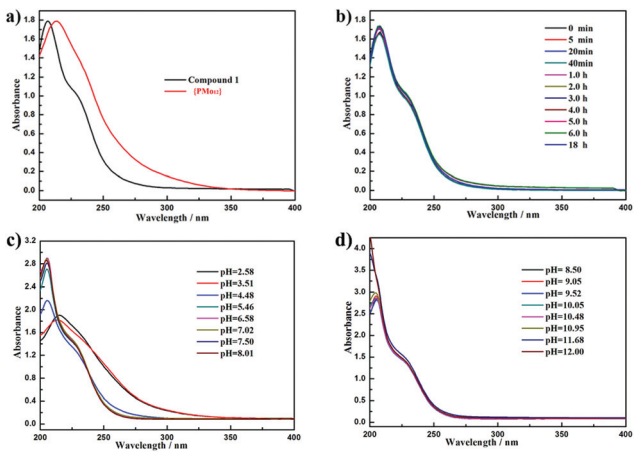

Fig. 3 (a) UV spectra of **1** (black) and $\{PMo_{12}\}$ (red) (2.5×10^{-5} mol L^{-1}); (b) UV spectra of **1** with time intervals; (c) and (d) UV spectra of **1** at different pH values.

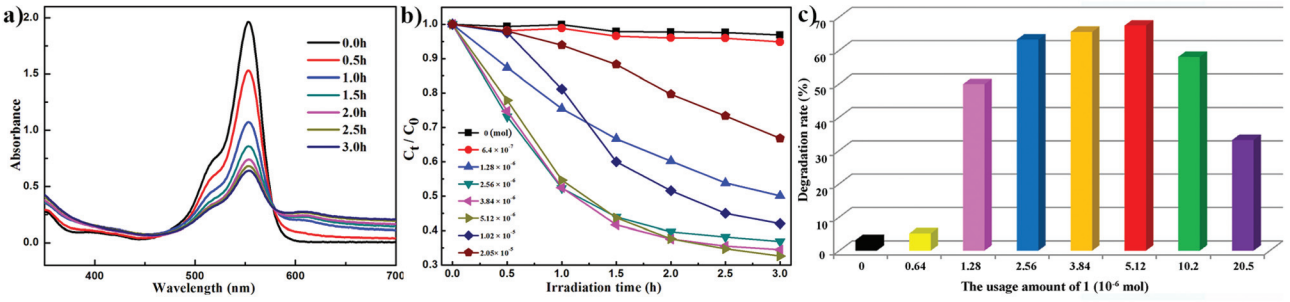

Fig. 5 (a) Absorption spectra of the RhB aqueous solution during the photodegradation under 500 W Xe-lamp irradiation in the presence of **1** at 5.12×10^{-6} mol; (b) photocatalytic decomposition of RhB solutions with the changes in C_t/C_0 *versus* irradiation time plot of **1** for 3.0 h; (c) degradation rates of RhB solutions with different amounts of **1**.

2.56×10^{-6}, 3.84×10^{-6}, 5.12×10^{-6}, 1.02×10^{-5} and 2.05×10^{-5} mol) identify that the optimum usage amount is 5.12×10^{-6} mol, and after irradiation for 3 h, the photocatalytic degradation rate, defined as $1 - C_t/C_0$, is 67.41% of **1** (Fig. 5c). The photocatalytic degradation rates are integrally presented in Table S7.† All in all, the photocatalytic activity is an important feature of complexes **1**, and it could be used to degrade some organic dyes.

Experimental section

Materials and methods

The precursor $Na_2HPMo_{12}O_{40}{\cdot}14H_2O$ was prepared according to the published procedure[24] and characterized by IR spectrum. All other chemical reagents were commercially purchased and used as received without any further purification. C, H and N elemental analyses were performed on an Elementar Vario MICRO analyzer. The IR spectra were obtained on a Bruker VERTEX 70 IR spectrometer (using KBr pellets) in the range of 4000–400 cm^{-1}. UV–vis absorption spectra were determined on a U-4100 spectrometer at room temperature. The TGA was carried out under a nitrogen gas atmosphere on a Mettler-Toledo TGA/SDTA851^e instrument from 25 to 900 °C with a heating rate of 10 °C min^{-1}.

XRPD measurement was performed on a Bruker AXS D8 Advance diffractometer instrument with Cu Kα radiation (λ = 1.54056 Å) in the angular range 2θ = 5–40° at 293 K. XPS spectra were recorded on a PHI5000 VersaProbe photoelectron spectroscope using monochromatic Al Kα radiation. The magnetic data were collected on a Quantum Design MPMS SQUID VSM magnetometer from 1.8 to 300 K at 1000 Oe.

Synthesis of $CsNa_9[H_2\{Ni_3O_2(H_2O)_6\}(PMo_6O_{21})_2(NiL_2)_3]{\cdot}21H_2O$ (1)

Solid $\{PMo_{12}\}$ (1.06 g, 0.50 mmol) and H_3L (0.30 g, 1.77 mmol) were dissolved in H_2O (10 mL), followed by the addition of solid $NiCl_2{\cdot}6H_2O$ (0.24 g, 1.01 mmol) and 0.25 mL 0.95 mol L^{-1} CsCl. When the pH of the reaction mixture was adjusted to about 6.0 using 6 mol L^{-1} NaOH, the turbid solution was heated to 80 °C for 2 h with constant stirring and the pH of the clear solution was about 6.1 at the end of the reaction. The solution was filtered after cooling to room temperature and the filtrate was left in an open beaker at room temperature. Blue block shape crystals of **1** were obtained after about three weeks. Yield: 0.26 g (38%) for **1** based on Ni. Elemental analysis (%) calcd for **1**: C, 5.28; H, 2.12; N, 2.05. Found: C, 5.27; H, 2.28; N, 1.95. The following abbreviations for selected IR (KBr, cm^{-1}) were used to assign the peak intensities: s, strong; m, medium; w, weak. 3430 (s), 2918 (m), 1583 (s), 1393 (w), 1333 (w), 1259 (w), 1215 (w), 1121 (s), 1067 (s), 1016 (m), 935 (s), 889 (s), 677 (s), 608 (w), 548 (w).

X-ray crystallography

Single crystal X-ray structure analysis was performed at 296 K on a Bruker Apex-II CCD diffractometer with graphite-monochromated Mo Kα radiation (λ = 0.71073 Å). The crystallographic data for **1** are listed in Table S5.† The structure of **1** was solved by direct methods and further refined by full-matrix least-squares refinements on F^2 using the SHELXL-97 software, and an applied multi-scan absorption correction was done using the SADABS program.[25] Routine Lorentz and polarization corrections were applied at the same time. In the final refinement, all the non-hydrogen atoms were refined anisotropically except for the disordered Na and water O atoms. Hydrogen atoms of organic groups were fixed in calculated positions and then refined using a riding model. All H atoms on water molecules were directly included in the molecular formula. CCDC reference number 1057128 is for **1**.

Conclusions

In summary, a simple and controllable one-pot reaction system was explored to prepare the novel hexa-nickel(II)-containing H_3L-functionalized heteropolyoxomolybdate. In the field of $Mo/O/RPO_3^{2-}$, the high TM-nuclear and the organic ligand synchronously incorporating into polyoxomolybdate in the present work is an important breakthrough. Meanwhile, the successful synthesis of **1** showed that this handy strategy can offer an effective way to make novel organophosphonate-decorated TM-contained polyoxomolybdate frameworks. Moreover, this work shed new light on the development of the

photocatalysts for the degradation of RhB solution, and magnetic studies indicate that compound **1** displays antiferromagnetic interactions.

In the future, different organophosphonate ligands with –COOH, $–NH_2$ and $–PO_3$ groups will be introduced into the present system to construct more novel frameworks and the roles of the organic components and TMs in the reactions are still being explored.

Acknowledgements

We gratefully acknowledge the National Natural Science Foundation of China, the Natural Science Foundation of Henan Province for financial support.

Notes and references

1 (*a*) C. Peloux, A. Dolbecq, P. Mialane, J. Marrot and F. Sécheresse, *Dalton Trans.*, 2004, 1259; (*b*) H. Q. Tan, W. L. Chen, D. Liu, Y. G. Li and E. B. Wang, *Dalton Trans.*, 2010, **39**, 1245; (*c*) H. Q. Tan, W. L. Chen, D. Liu, X. J. Feng, Y. G. Li, A. X. Yan and E. B. Wang, *Dalton Trans.*, 2011, **40**, 8414; (*d*) N. Calin and S. C. Sevov, *Inorg. Chem.*, 2003, **42**, 7304; (*e*) J. D. Compain, P. Mialane, J. Marrot, F. Sécheresse, W. Zhu, E. Oldfield and A. Dolbecq, *Chem. – Eur. J.*, 2010, **16**, 13741; (*f*) H. E. Moll, A. Dolbecq, I. M. Mbomekalle, J. Marrot, P. Deniard, R. Dessapt and P. Mialane, *Inorg. Chem.*, 2012, **51**, 2291; (*g*) A. Dolbecq, P. Mialane, F. Sécheresse, B. Keita and L. Nadjo, *Chem. Commun.*, 2012, **48**, 8299; (*h*) A. Proust, R. Thouvenot and P. Gouzerh, *Chem. Commun.*, 2008, 1837.

2 (*a*) W. Kwak, M. T. Pope and T. F. Scully, *J. Am. Chem. Soc.*, 1975, 5735; (*b*) J. Stalick and C. Quicksall, *Inorg. Chem.*, 1976, **15**, 1577; (*c*) M. Carraro, U. Kortz and M. Bonchio, *Angew. Chem., Int. Ed.*, 2008, **47**, 7275.

3 (*a*) A. Dolbecq, L. Lisnard, P. Mialane, J. Marrot, M. Bénard, M. Rohmer and F. Sécheresse, *Inorg. Chem.*, 2006, **45**, 5898; (*b*) K. P. Rao, V. Balraj, M. P. Minimol and K. Vidyasagar, *Inorg. Chem.*, 2004, **43**, 4610; (*c*) R. C. Finn, R. S. Rarig and J. Zubieta, *Inorg. Chem.*, 2002, **41**, 2109; (*d*) E. Burkholder, V. Golub, C. J. O'Connor and J. Zubieta, *Chem. Commun.*, 2003, 2128; (*e*) N. G. Armatas, D. G. Allis, A. Prosvirin, G. Carnutu, C. J. O'Connor, K. Dunbar and J. Zubieta, *Inorg. Chem.*, 2008, **47**, 832; (*f*) X. P. Sun, D. H. Yang, G. G. Wang, Z. J. Liang, P. T. Ma, J. P. Wang and J. Y. Niu, *RSC Adv.*, 2015, **5**, 31392; (*g*) E. Dumas, C. Sassoye, K. D. Smith and S. C. Sevov, *Inorg. Chem.*, 2002, **41**, 4029; (*h*) H. E. Moll, W. Zhu, E. Oldfield, A. Dolbecq, *et al.*, *Inorg. Chem.*, 2012, **51**, 7921.

4 L. Yang, P. T. Ma, Z. Zhou, J. P. Wang and J. Y. Niu, *Inorg. Chem.*, 2013, **52**, 8285.

5 (*a*) U. Kortz, C. Marquer, R. Thouvenot and M. Nierlich, *Inorg. Chem.*, 2003, **42**, 1158; (*b*) X. M. Li, Y. G. Chen, C. N. Su, S. Zhou, Q. Tang and T. Shi, *Inorg. Chem.*, 2013, **52**, 11422; (*c*) W. N. Wang, J. Li, Z. G. Sun, F. Tong, Y. Y. Zhu, L. Xu and J. Gong, *Z. Anorg. Allg. Chem.*, 2011, **637**, 108; (*d*) P. DeBurgomaster, A. Aldous, H. X. Liu, C. J. O'Connor and J. Zubieta, *Cryst. Growth Des.*, 2010, **10**, 2209.

6 (*a*) N. G. Armatas, W. Ouellette, K. Whitenack, J. Pelcher, H. X. Liu, E. Romaine, C. J. O'Connor and J. Zubieta, *Inorg. Chem.*, 2009, **48**, 8897; (*b*) E. Burkholder, V. Golub, C. J. O'Connor and J. Zubieta, *Inorg. Chem.*, 2003, **42**, 6729.

7 L. Yang, Z. Zhou, P. T. Ma, J. P. Wang and J. Y. Niu, *CrystEngComm*, 2013, **15**, 5452.

8 (*a*) X. J. Dui, W. B. Yang, X. Y. Wu, X. F. Kuang, J. Z. Liao, R. M. Yu and C. Z. Lu, *Dalton Trans.*, 2015, **44**, 9496; (*b*) Q. Wu, W. L. Chen, D. Liu, C. Liang, Y. G. Li, S. W. Lin and E. B. Wang, *Dalton Trans.*, 2011, **40**, 56; (*c*) Y. Hu, H. Y. An, X. Liu, J. Q. Yin, H. L. Wang, H. Zhang and L. Wang, *Dalton Trans.*, 2014, **43**, 2488; (*d*) M. Najafi, A. Abbasi, M. Masteri-Farahani and J. Janczak, *Dalton Trans.*, 2015, **44**, 6089.

9 L. J. Zhang, S. Xu, Y. S. Zhou, X. R. Zheng, C. Yu, Z. H. Shi, S. Hassan and C. Chen, *CrystEngComm*, 2011, **13**, 6511.

10 P. H. Smith, F. E. Hahn, A. Hugi and K. N. Raymond, *Inorg. Chem.*, 1989, **28**, 2052.

11 H. E. Moll, A. Dolbecq, J. Marrot, G. Rogez, M. Haouas, F. Taulelle, G. Rogez, W. Wernsdorfer, B. Keita and P. Mialane, *Chem. – Eur. J.*, 2012, **18**, 3845.

12 Y. Huo, Z. Y. Huo, P. T. Ma, J. P. Wang and J. Y. Niu, *Inorg. Chem.*, 2015, **54**, 406.

13 L. Yang, Y. Huo and J. Y. Niu, *Dalton Trans.*, 2013, **42**, 364.

14 U. Kortz, J. Vaissermann, R. Thouvenot and P. Gouzerh, *Inorg. Chem.*, 2003, **42**, 1135.

15 M. Ramstedt, C. Norgren, J. Sheals, D. Boström, S. Sjöberg and P. Persson, *Inorg. Chim. Acta*, 2004, 1185.

16 I. D. Brown and D. Altermatt, *Acta Crystallogr.*, 1985, **B41**, 244.

17 (*a*) M. Yuan, Y. G. Li, E. B. Wang, Y. Lu, C. W. Hu, N. H. Hu and H. Q. Jia, *Dalton Trans.*, 2002, 2916; (*b*) Q. H. Geng, Q. S. Liu, P. T. Ma, J. P. Wang and J. Y. Niu, *Dalton Trans.*, 2014, **43**, 9843.

18 L. Raki and C. Detellier, *Chem. Commun.*, 1996, 2475.

19 Y. N. Zhang, B. B. Zhou, Y. G. Li, Z. H. Su and Z. F. Zhao, *Dalton Trans.*, 2009, 9446.

20 B. Modec, D. Dolenc and M. Kasunič, *Inorg. Chem.*, 2008, **47**, 3625.

21 J. Y. Niu, J. A. Hua, X. Ma and J. P. Wang, *CrystEngComm*, 2012, **14**, 4060.

22 B. S. Bassil, M. Ibrahim, S. S. Mal, A. Suchopar, R. N. Biboum, B. Keita, L. Nadjo, S. Nellutla, J. V. Tol, N. S. Dalal and U. Kortz, *Inorg. Chem.*, 2010, **49**, 4949.

23 (*a*) K. Hakouk, P. Deniard, L. Lajaunie, Z. Wang, H. Koo, M. H. Whangbo and R. Dessapt, *Inorg. Chem.*, 2013, **52**, 6440; (*b*) L. Wang, W. T. Yang, W. Zhu, X. G. Guan, Z. G. Xie and Z. M. Sun, *Inorg. Chem.*, 2014, **53**, 11584; (*c*) H. Y. An, Y. Hu, L. Wang, E. L. Zhou, F. Fei and Z. M. Su, *Cryst. Growth Des.*, 2015, **15**, 164; (*d*) M. T. Li, J. Q. Sha, X. M. Zong, J. W. Sun, P. F. Yan, L. Li and X. N. Yang, *Cryst.*

Growth Des., 2014, **14**, 2794; (*e*) X. X. Xu, X. Gao, Z. P. Cui, X. X. Liu and X. Zhang, *Dalton Trans.*, 2014, **43**, 13424; (*f*) X. Meng, C. Qin, X. L. Wang, Z. M. Su, B. Li and Q. H. Yang, *Dalton Trans.*, 2011, **40**, 9964; (*g*) Q. Lan, J. Zhang, Z. M. Zhang, Y. Lu and E. B. Wang, *Dalton Trans.*, 2013, **42**, 16602; (*h*) Q. Lan, Z. M. Zhang, Y. G. Li, Y. Lu and E. B. Wang, *Dalton Trans.*, 2014, **43**, 16265.

24 C. Rocchiccioli-Deltcheff, M. Fournier, R. Franck and R. Thouvenot, *Inorg. Chem.*, 1983, **22**, 207.

25 (*a*) G. M. Sheldrick, *SHELXS97, Program for Crystal Structure Solution*, University of Göttingen, Göttingen, Germany, 1997; (*b*) G. M. Sheldrick, *SHELXL2014, Program for Crystal Structure Refinement*, University of Göttingen, Göttingen, Germany, 2014.